Membrane mirrors for vision science adaptive optics

Peter Kurczynski[a,b], J. Anthony Tyson[a], Bernard Sadoulet[b], David Bishop[a], David R. Williams[c]
[a]Bell Laboratories, Lucent Technologies, Murray Hill, NJ 07049
[b]University of California Berkeley, Berkeley, CA 94720
[c]Center for Visual Sciences, University of Rochester, Rochester, NY 14627

ABSTRACT

Adaptive optics provides a means to measure and correct aberrations in human vision. This technology is being used to diagnose vision problems, study the mechanism of human vision, and extend the capabilities of nature's optics. The ideal wavefront corrector for vision science adaptive optics would have greater stroke, and more degrees of freedom than is currently available. Micromachined deformable mirrors may soon meet these demands. Membrane mirrors in particular offer a promising alternative to other MEMS deformable mirror designs. A new type of mirror, employing a bound charge layer on the membrane, may overcome some of the limitations of previous membrane mirrors.

Keywords: adaptive optics, MEMS, MOEMS, optical MEMS, micromirrors, deformable mirrors, ocular aberrations

1. ABERRATIONS TO HUMAN VISION

Human vision is subject to optical aberrations that have been measured and corrected with adaptive optics. Defects of defocus and astigmatism can be partially corrected with spectacles and contact lenses. Ocular aberrations include higher order[1], irregular aberrations that are unique to human vision. Refractive errors are known to occur at the first surface of the cornea, and at other surfaces of the cornea and lens. They vary from individual to individual, however they are not random defects. These aberrations can severely impair the vision of some individuals; kerataconus is a disease in which the cornea takes on a cone shape resulting in severe high order aberrations. The correction of these aberrations works for light going in either direction, and would thus benefit ophthalmic studies as well as vision correction.

Even the eyes of persons with uncorrected vision fall short of diffraction limited performance, particularly when the pupils are dilated [1]. Figure 1 illustrates the wavefront error as a function of Zernike polynomial order averaged from a sample of 14 human eyes. An RMS error of $< \lambda/14$ (0.045 μm at 0.633 μm measurement wavelength) is a commonly used criterion for diffraction limited optical performance. This level of error is indicated as a dashed line in Figure 1. At the dilated pupil size of 7.3 mm, wavefront errors exceed this tolerance for all Zernike polynomials up to eighth order. For comparison, these data include wave aberrations of an "artificial eye" consisting of an achromatic doublet (f=16 mm) and a diffuser. Although the artificial eye exhibits some spherical aberration (Zernike order 4), comparison with the data from living eyes reveal that nature's optics are an order of magnitude worse for nearly each Zernike order.

Vision science applications of adaptive optics are just being explored; recent progress is reviewed in [2] and [3]. Adaptive optics has been used to image individual cells of the living retina to study color vision [4]. Such high resolution imaging may permit early detection and possibly treatment of diseases that affect the retina including glaucoma and microaneurysms caused by diabetes [3]. Adaptive optical systems can be used to test in advance the effects of refractive surgery. Measurements enabled by wavefront sensing will enable the customized correction of high order optical aberrations through refractive surgery and improved contact lenses [5].

[1] Optical aberrations are commonly described by an expansion of the phase of the optical wavefront over a set of orthogonal functions, such as Zernike polynomials.

2. ADAPTIVE OPTICS

Adaptive optics uses a wavefront sensor to measure phase aberrations in an optical system, and a deformable mirror or other wavefront compensating device to correct these aberrations. The present technology evolved from the need to correct for aberrations in ground based telescope images caused by atmospheric turbulence; the history of this technology and its application to astronomy are reviewed in [6] [7] [8] [9]. Essential components to an adaptive optics system include the wavefront sensor, deformable mirror, and appropriate control hardware and software.

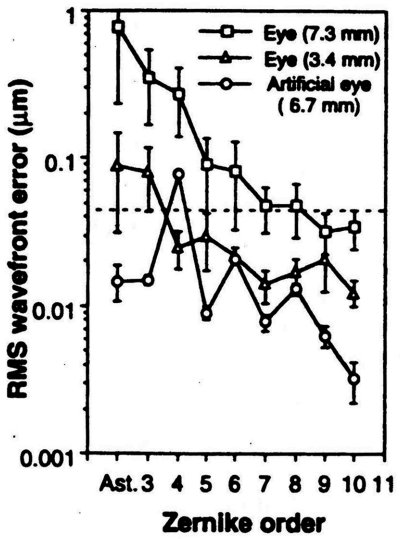

Figure 1. RMS wavefront error vs. Zernike polynomial order measured from a sample of normal human eyes. Wavefront aberrations for dilated pupils (7.3 mm) are plotted with squares. Un-dilated pupil (3.4 mm) data are plotted with triangles. For comparison, wave aberrations from an artificial eye are plotted with circles. The horizontal, dashed line denotes the RMS wavefront error for diffraction limited optical performance. Data reproduced from [10].

A variety of wavefront sensing schemes have been employed; these are reviewed in [11]. The Shack-Hartman sensor, a widely used design, detects aberrations from a plane wave by tracking deviations in image positions of an array of spot images formed by a lenslet array. A plane wavefront incident on the lenslet array creates a regular grid of spots at the image plane. The spot positions wander in the image plane in response to a varying optical phase at the entrance pupil. The measured spot deviations correspond to the gradient of this optical phase. Curvature sensing, another common approach, extracts phase information from the difference of two images defocused by a known amount. As the name implies, curvature sensing directly measures the curvature of the wavefront, which can be related to the Laplacian of the phase function [12]. As discussed in Section 4.7, this feature makes curvature sensors especially useful for membane mirrors.

A plethora of techniques have been applied to wavefront compensation. Most of these approaches use mirrors that deform to introduce path length changes across the pupil to bring the reflected wavefront into phase; deformable mirrors are reviewed in [13]. Position dependent changes in the index of refraction of a transmissive medium can also compensate for phase aberrations. This principle underlies the operation of liquid crystal wavefront correctors, which are reviewed in [14].

Deformable mirrors may be broadly categorized as either continuous face sheet, membrane, or segmented. Design tradeoffs among the various types of deformable mirror, excluding microfabricated mirrors, are discussed in [15] [16].

Continuous face sheet mirrors were the first type to be implemented in working systems. They consist of a thin deformable mirror surface that is controlled by an array of actuators underneath this surface. The mirror stroke is defined as the linear range of motion of the deformable mirror. The influence function refers to the influence on the surrounding parts of the mirror due to actuation of a single actuator; influence function may be quoted as a percentage of central actuator displacement experienced by nearest neighbor actuators. Piezoelectric or electrostrictive actuators can push or pull selected points of attachment on the mirror. Currently, Xinetics Inc., supplies piezoelectric deformable mirrors that have ±1μm stroke and ~10% influence functions.

Several research groups have fabricated continuous face sheet deformable mirrors using surface micromachining [17], and bulk micromachining [18]. These devices are actuated by electrostatic attraction operating against mechanical restoring forces. Surface micromachined devices are popular in part due to the availability of commercial processes such as the Multi User MEMS Process (MUMPs) of JDS Uniphase MEMS Business Unit. MUMPs is a three layer polysilicon micromachining process that uses alternating layers of polysilicon (the structural material), and oxide (the sacrificial material), on a silicon nitride insulating layer. Deformable mirrors, designed at Boston University and fabricated through MUMPs, are being investigated for their application to vision science adaptive optics; these mirrors have narrow influence functions (~10%), and high resonant frequency. However, design rules of the MUMPs process limit the stroke that may be achieved with such devices to less than 2 μm. Print through of underlying layers and etch holes in the top surface impact the optical quality of surface micromachined devices. Curvature due to residual material stresses can impair performance. Investigators have applied various novel approaches to addressing and circumventing these limitations [19].

Higher stroke actuation may be achieved with bulk micromachined devices. In such devices, electrode and mirror may be fabricated on separate dies, and wafer bonded together. This approach adds flexibility to the design process. Examples of these devices include mirrors made at Stanford University and Intellite Corporation [18].

Membrane mirrors, consisting of thin, tensioned membranes that are supported only at the periphery, are discussed in detail in Section 4. One variant of this type of mirror includes the bimorph piezoelectric mirrors, which consist of two thin layers of oppositely poled piezoelectric material, with actuating electrodes sandwiched in between [20]. Such mirrors have been used in astronomical adaptive optical systems.

Segmented mirrors consist of an array of individually controlled segments, or facets. Segmented mirrors have advantages of low operating voltages, compared to continuous devices, and high resonant frequencies. Segmented mirrors exhibit no spatial cross-talk. Influence functions are step functions, in contrast to the broader gaussian functions that are typical of continuous face-sheet mirrors, and the logarithmic influence functions that are typical of membrane mirrors. For monochromatic applications, segmented mirrors require as little as ± ½λ stroke to operate effectively. Discontinuous phase steps that occur within the pupil area will phase correctly if the steps are made at integer numbers of wavelengths. This procedure, known as phase wrapping, is ineffective for broadband applications.

To offset the advantages of segmented mirrors, these devices exhibit less than 100% fill factor. As a result, some incident energy is lost, and diffraction from support structures and edges of individual pixel elements increases [21]. One novel approach to these problems consists of placing lenslet arrays in the optical path to focus light onto the segmented mirror surfaces [22].

Segmented mirrors with piston and tip/tilt capability on individual segments have been made with piezoelectric actuators [23]. Segmented, micromachined mirrors have been designed for adaptive optics applications. Mirrors with piston and tip/tilt capability were designed by Air Force research groups and fabricated according to the MUMPs and SUMMiT (Sandia Ultra Planar Multi-level MEMS Technology) standards [24] [25].

Vision science adaptive optics demands more stroke from MEMS mirrors than is possible with MUMPs or SUMMiT processes. In one promising device, bimorph flexure was used to lift actuator structures out of the plane to enable larger stroke, segmented devices from a surface micfromachined fabrication process [26]. Residual stresses are designed into nickel-polysilicon support flexures that elevate mirror bond pads 20 μm above the electrode plane after release. This process enables the device to achieve 6 μm stroke with piston and tip/tilt capability. In this novel device, mirrors are

attached to each segment of the MEMS chip through fluidic self assembly. Self assembly occurs when the device is immersed in a liquid bath containing many mirror segments. Capillary forces on individual mirror segments cause them to align with bond sites on the elevated bond pads [27].

3. REQUIREMENTS OF A VISION SCIENCE ADAPTIVE OPTICS SYSTEM

Vision science adaptive optical systems operate in broad band visible light, and ideally will correct aberrations at video frame rates (30 Hz). In order to preclude the use of long relay optics in an adaptive optics system, deformable mirrors should ideally match the diameter of a dilated human pupil. For commercial applications, devices must be compact and relatively inexpensive. These requirements favor micromachined devices as one design solution.

A deformable mirror designed for vision science applications must deliver sufficient stroke to correct the aberrations of the human eye. Low Zernike order aberrations dominate the total aberration in human vision. For example, residual defocus, defined as the amount of defocus remaining when vision is corrected to 20/20, accounts for 60-65% of aberrations in normal human eyes. Correcting for these low order aberrations in all individuals may require 8 μm stroke [28]. As illustrated in Figure 1, a sample of normal human eyes exhibits 0.8 μm RMS wavefront error in 2nd order Zernike modes (astigmatism). This error corresponds to a peak to valley wavefront aberration of 3.2 μm, and a mirror stroke of 1.6 μm to provide adequate correction. Additional data are tabulated in Table 1. Correspondingly less mirror stroke is required at higher Zernike orders and thus at higher spatial frequencies.

Zernike Order	**RMS Wave-Front Error**	**PV Wave-Front Error**	**Mirror Stroke**
2 (Astigmatism)	0.8 μm	3.2 μm	1.6 μm
3	0.35 μm	1.4 μm	0.7 μm
4	0.27 μm	1.1 μm	0.6 μm
10	0.035 μm	0.14 μm	0.07 μm

Table1: Representative root mean square (RMS) and peak to valley (PV) wavefront errors from a sample of normal human eyes, and corresponding mirror stroke required for correction. RMS Wavefront Error X 4 = PV Wavefront Error. PV Wavefront Error / 2 = Mirror Stroke. Data from [10]

Simulations of various deformable mirror types have begun to address the number of segments (for segmented deformable mirrors) or control electrodes (for continuous deformable mirrors) required to achieve diffraction limited optical performance [29]. Figure 2 illustrates the Strehl[2] ratio vs. facet number from a segmented deformable mirror model that simulated correction to wave aberration data from a sample of normal eyes. The upper curves consist of Strehl ratios computed for data with residual defocus and astigmatism removed, while the lower two curves include residual defocus and astigmatism in the total wave aberration. Residual defocus and astigmatism are singled out because some adaptive optics systems may correct these aberrations with a separate tip/tilt mirror. Higher Strehl ratios can be achieved with fewer facets if residual defocus and astigmatism are removed. Taken together, both sets of curves illustrate the dominating influence of residual defocus and astigmatism on the overall aberration.

This deformable mirror model assumes piston only motion, 100% fill factor, and negligible diffraction from inter-facet support structures. The two sets of curves in Figure 2 demonstrate that diffraction limited performance, Strehl > 0.8, requires 20-50 facets across the 6.0 mm (average) pupil. In correcting for atmospheric turbulence, continuous

[2] Strehl ratio is defined as the ratio of peak intensity of the point spread function to the intensity of a corresponding, diffraction limited point spread function. Strehl ratio > 0.8 is one criterion for diffraction limited performance.

deformable mirrors require fewer degrees of freedom than segmented mirrors to achieve the same fitting error [30]. Almost undoubtedly, a similar relationship holds for correcting aberrations to vision; hence these facet numbers set an upper bound for the required number of electrodes across the pupil of a continuous deformable mirror. The two curves comprising each upper and lower pair in Figure 2 refer to different electrode shapes. Their similarity suggests that electrode shape is of only secondary importance in achieving diffraction limited wavefront correction.

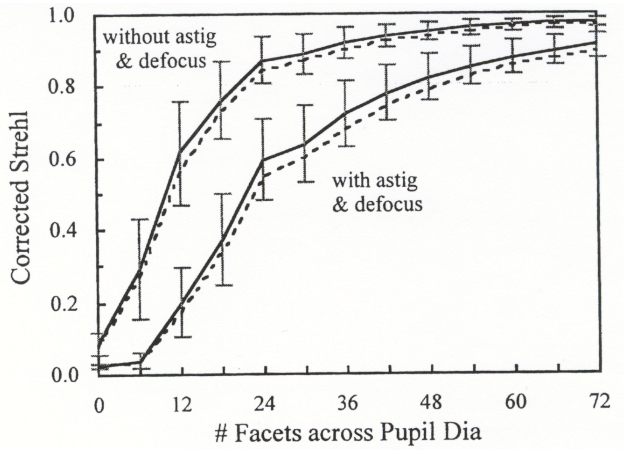

Figure 2. Corrected Strehl ratio for (solid) hexagonally- and (dashed) square-packed SLM configurations as a function of segment number. Pupil diameter and λ were set to 6 mm and 0.6 μm, respectively. Top two curves have defocus and astigmatism removed. Bottom two curves contain the residual amount of defocus and astigmatism uncorrected by trial lenses. Error bars represent ±1 standard deviation across the 12 subjects. Figure reproduced from [29].

4. MEMBRANE DEFORMABLE MIRRORS

4.1 Overview

Deformable mirrors made from tensioned membranes were considered early on as a wavefront corrector for adaptive optics [31]. The membrane must have an optically flat, reflecting surface. It is mechanically supported at its periphery and suspended a fixed distance above an actuating electrode plane. Prior to micromachined adaptive optical systems, various designs used membranes made of titanium and other materials [32] including mylar [33], and nitrocellulose [34] [35].

More recently, membrane mirrors have been designed by Gleb Vdovin and are commercially available through Flexible Optical BV (OKO Technologies). These membranes, made of silicon nitride, have been fabricated using bulk silicon micromachining techniques [36]. Silicon nitride was originally chosen because it is mechanically strong, an insulator, it can be fabricated with known stress, and it is not etched in KOH. To fabricate the mirrors, a 0.5 μm thick layer of silicon nitride was deposited onto a silicon wafer; this wafer was subsequently etched in KOH to release the membranes. A ~200 nm thick aluminum layer was deposited on the membranes to enhance reflectivity. Membranes were square, between 10 and 15 mm wide. Membrane stress was measured to be ~50 MPa. Membranes were suspended 40 μm over an actuating electrode array containing between 9 and 37 hexagonal, actuating electrodes. As discussed in detail below, the membrane mirrors deform due to electrostatic attraction of the metallized membrane to selectively charged electrodes. Various groups have used membrane mirrors from Flexible Optical BV (OKO Technologies) for vision science adaptive optics [37] [38], correction of atmospheric turbulence [39], confocal microscopy [40], adaptive laser wavefront correction [45], and as aberration generators to study the capabilities of membrane mirrors for correcting atmospheric turbulence [41] and human vision [42].

Other research groups have fabricated membranes made of silicon nitride [43], single crystal silicon [44], polysilicon [45], and polyimide [46]. To date, membrane mirrors have been designed with a few tens, but so far not hundreds, of

electrodes actuating the membrane surface. Electrostatic attraction provides the most common, though not exclusive, means of controlling the mirror shape.

Magnetically actuated membranes have been investigated for adaptive optics applications [46][47]. Magnetic actuation has been achieved using miniaturized current coils, fabricated on a separate wafer, acting on permanent magnets affixed to the membrane. Polyimide membranes were formed by spin coating one or more layers onto a GaAs substrate. The wafers were baked, and subsequently wet etched to release the membranes from the GaAs. Membranes were made with 1.5-15 μm thickness, 11.5 MPa stress; these parameters enabled high stroke deformation in the completed devices. Resonant frequency was measured at 485 Hz. In one prototype, 19 permanent magnets, 1mm diameter, were affixed to the underside of the membrane, which was mounted 150 μm above an actuating coil wafer. This device demonstrated ~20 μm single actuator stroke. Thin magnetic films sputtered onto the membrane may replace permanent magnets as this membrane concept matures.

To minimize ohmic heating, high aspect ratio current coils have been fabricated using the LIGA (Lithographie, Galvanofornung & Abformung : Lithography, Electroplating & Molding) process. In this process, lithography is achieved in a polymer resin by exposure to UV or X-ray radiation through a patterned, metal mask. The resin acts as a mold that is filled with metal by electroplating. Structures as thick as 1mm can be fabricated with micron precision. A prototype coil array fabricated in this way may consist of ~1 mm diameter coils composed of 80-100 μm deep, 80 μm wide copper wire separated by a 20 μm gap. Such coils can withstand currents in excess of 2A. A cooling system may not be required except for infrared applications. Notably, these membrane devices exhibit a linear mechanical response as a function of actuating current (6.6 μm/A) over a ± 2.5A range.

Generally, analog voltages (in the case of electrostatic membranes) or currents (for magnetic membranes), commanded to each electrode cause the membrane mirror to deform to a desired shape. Alternatively, electrostatic actuation using multiple digital signals to a concentric ring of sub-actuators has been explored with promising results [48]. Analog designs use a separate digital to analog converter for each electrical channel. Deformable mirrors with many tens or hundreds of actuators would thus require large racks of discrete electronics to drive them. This practical consideration provides a limitation that has recently been relieved with the commercial availability of drive electronics manufactured at Lucent Technologies, and now available through Agere. In micromachined systems, digital to analog conversion may ultimately be performed underneath the electrode, using ASICs on the same chip, and several groups are pursuing this approach.

4.2 Basic Principles of Membrane Mirror Design

A membrane is a special case of an elastic thin plate, whose theory has been extensively studied [49] [50]. Let the height of the mid-plane of the plate be described by the function, ξ, of two coordinates in the plane of the plate. The static equilibrium shape of a thin plate subject to deflections that are large compared to its thickness, but small compared to its length, is described by a fourth order differential equation in ξ that relates stresses due bending, elasticity and external forces [51].

In this context, a membrane is defined as a plate whose thickness is very small compared to its diameter. For a membrane that is clamped at its periphery and held under a uniform tension per unit length, *T*, the fourth order plate bending equation becomes a Poisson equation

$$\nabla^2 \xi = -\frac{P}{T} \qquad [1]$$

P is the lateral pressure experienced by the membrane. It has been shown experimentally that this membrane model is appropriate for structures whose length exceeds their thickness by factors of 1000 or more, typical of membrane mirrors [52]. This model becomes inaccurate at very high amplitudes or spatial frequencies, as bending stresses become comparable to the elastic stress due to tension; however, these extremes are not encountered in practice.

In membranes made from a stretched film, the tension must be applied mechanically during assembly. For microfabricated membranes that are fabricated by bulk etching a wafer to release the membrane, tension is related to the material stress, S, and the thickness, h, as $T = S\,h$.

In electrostatic membrane devices, each electrode forms a parallel plate capacitor with the membrane surface. Accordingly, the electrostatic attractive force due to a single electrode, energized to a voltage, V, results in a localized pressure on the membrane approximately given by

$$P = \frac{1}{2}\varepsilon_0 \frac{V^2}{d^2} \qquad [2]$$

d is the distance between the electrode and the membrane. As the membrane-electrode distance decreases, the electrostatic pressure increases, and finally dominates any other restoring forces, such as tension. This phenomenon is well known in MEMS design, and leads to the 1/3 gap instability, whereby electrostatic actuation is stable only for deflections less than 1/3 the distance from the moveable element to the electrode. Larger deflections will cause the membrane to snap down to the electrode surface.

Inserting Equation [2] into Equation [1] yields a nonlinear equation for the static equilibrium shape of the membrane:

$$\nabla^2 \xi = -\frac{\varepsilon_0 V^2}{2T\left(d_0 - \xi\right)^2} \qquad [3]$$

d_0 is the distance between the undeformed, flat membrane and the electrode plane. For small deformations from a flat mirror shape, the right hand side may be expanded in a power series in ξ/d_0. Neglecting second order and higher order terms yields

$$\nabla^2 \xi = -\frac{\varepsilon_0 V^2}{2T d_0^{\,2}} \qquad [4]$$

Equation [3] or [4], can be solved to predict the membrane deformation from known actuator voltages. In modeling membrane mirrors from Flexible Optical BV (OKO Technologies), the linear approximation may lead to errors of ~10% for predicted quantities.

4.3 Restoring Force

Electrostatic pressure can only attract the membrane to the electrode, as illustrated by the dependence of this pressure on the square of the voltage in Equation [2]; changing the sign of the voltage has no effect on the pressure. To enable actuation of the membrane in both directions (push and pull) several approaches have been explored. In one design, a transparent electrode was placed some distance above the membrane, in the optical path [32]. Electrostatic attraction to this bias electrode provided a restoring force to the membrane. This attractive force contributes an extra term to the pressure, opposite in sign to that due to actuating electrodes, in Equation [2]. The bandwidth limitation imposed by transmission through the transparent electrode and window is not necessarily restrictive for vision science. A new membrane mirror approach, discussed below, could make use of such a transparent bias electrode.

Magnetic (current actuated) membrane mirrors can deform in both directions without the use of a bias electrode, by changing the sign of the current in the actuating coils. As discussed previously, membrane displacement due to magnetic actuation is linear in the applied current over a wide range of currents.

Flexible Optical BV (OKO Technologies) mirrors are pre-biased to a concave, spherical shape. This bias curvature introduces a known, weak positive optical power into the system. The necessary voltages to deform the mirror to this shape can be found through an optimization procedure using a pinhole reference source [52]. Releasing regions of the

mirror from the bias curvature is equivalent to repulsion away from the electrode over a limited range defined by the envelope of the bias curvature.

It may be noted that a membrane under constant (over the membrane surface) pressure deforms to a paraboloid, as can be seen by solving Equation [1] with P held constant over the membrane surface. In practice, edge non-uniformities in the membrane tension may introduce astigmatism in micromachined membranes when a constant pressure is applied to the membrane.

4.4 Influence Function

Using the membrane model embodied in Equation [4], analytical and numerical calculations demonstrate the capability of membrane mirrors to deliver high stroke actuation, as required by vision science applications. Figure 3 illustrates an analytical solution of Equation [4] for a circular membrane, radius a, subject to lateral pressure from a single, centered actuator of radius $a/18$. A membrane with thickness h=0.4 μm and stress, S=10 MPa yields a tension T = 4 N/m^2. With a membrane-electrode distance d_0=40 μm and an actuating voltage V=200 V, a maximum stroke of 14 μm is achieved. Numerical solution of Equation [4], using a Gauss-Seidel iteration scheme, for a rectangular membrane, yielded similar results. This amount of stroke is enabled by two factors: a thin, low stress membrane reduces tension, and a small gap between membrane and electrodes increases the electrostatic pressure. These calculations demonstrate the importance of membrane stress and thickness in determining the maximum amount of mirror deformation. High stroke actuation requires low (10-50 MPa) stress membranes.

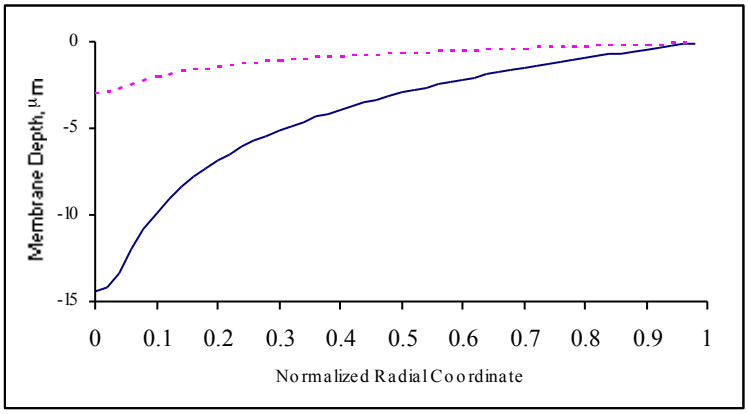

Figure 3. Electrostatic deformation of membranes can yield large stroke. These curves illustrate the deformation of membranes under electrostatic attraction to a single, energized electrode at the center (r=0). Electrode radius = 0.05 (scaled with respect to membrane radius). Electrode voltage = 200 V, membrane-electrode distance = 40μm. Membrane stress is 10 MPa (solid curve) and 50 MPa (dashed curve).

Figure 3 also illustrates the global nature of the deformation due to a single actuator, a characteristic of membrane mirrors. Unlike segmented mirrors, whose segments can be actuated independently, or continuous face-sheet mirrors, which exhibit localized deflections, membrane mirrors have broad influence functions. This characteristic is not necessarily an impediment to their performance in an adaptive optical system, and is in many cases an advantage, as will be discussed in Section 4.8.

4.5 Electrode Array Geometry

Silicon microfabrication of electrode arrays will permit greater flexibility in the number, size and geometry of electrodes than has been realized to date. Some research has addressed the optimum design and placement of electrodes underneath the membrane mirror.

The supporting frame constrains the edges of the membrane, hence electrodes placed underneath the periphery of the membrane will have little actuating effect. Accordingly, if the entire membrane is used in the optical system, the membrane mirror will be unable to reproduce shapes, such as Zernike polynomials, that require large deflections at the edge of the pupil.

To correct this deficiency, the active optical area of the membrane mirror should consist of only the central portion of the membrane, where the membrane is not constrained by its supporting frame. One numerical study found an optimum pupil diameter of 65% of the membrane diameter for the correction of atmospheric turbulence [39].

Membrane mirrors have been controlled with hexagonal electrode arrays, electrodes that are sections of concentric rings, and other geometries. In the simplest electrode array designs, the electrode plane is tiled with electrodes of equal area. This approach is not ideal however, since the effectiveness of particular electrodes for deforming the mirror surface depends on their location under the membrane. For a given actuating voltage, electrodes near the edge of the membrane would require larger area to exert the same influence on the membrane shape as electrodes near the center. A method for designing electrode configurations that equalizes the peak mirror deformation for each electrode is presented in [53]. This method incorporates nonlinearity of the membrane deformation demonstrated in Equation [3], and hence has broad applicability.

4.6 Dynamic Response

The bandwidth of a closed loop adaptive optics system may be limited by the resonant frequency of the deformable mirror. Resonant frequencies of the deformable mirror should exceed the maximum closed loop operating frequency by at least a factor of ten. Vision science applications prefer closed loop operation at 30 Hz; therefore, membrane resonant frequencies should exceed 300 Hz.

In the absence of external forces such as those provided by air pressure, the dynamic response of a membrane under tension is described by the wave equation in two dimensions. Resonant frequencies can be found as eigenvalues of this equation. The resonance frequencies, $f_{k,m}$, in Hz, of a circular membrane, radius a, mass density, σ, under tension/length, T, are derived in [54]

$$f_{k,m} = \frac{1}{2\pi a}\alpha_{k,m}\sqrt{\frac{T}{\sigma}} \qquad [5]$$

$\alpha_{k,m}$ is the m'th root of a Bessel function of order k. Using Equation [5], resonance frequencies for an 8.0 mm radius, silicon nitride membrane (density between 1.0 and 2.0 g/cm^3), 0.4 μm thick, with 20 MPa stress, are all above 4.8 kHz. Higher stress membranes have higher frequencies of resonance. This example ignores the effect of pressure changes occurring within the enclosed vessel behind the membrane due to air trapping.

Air trapping increases the resonant frequencies of the membrane and vessel, compared to that of the membrane in vacuum [55]. Therefore, if the membrane vessel is enclosed, the pressure of air within the vessel may be tuned to place the resonant frequency outside the dynamic range of the intended closed loop application. Grosso and Yellin employed this technique to achieve membrane plus vessel resonant frequencies as high as 8 kHz [32].

Air pressure within the vessel provides a damping force to the membrane. In vacuum, a membrane is undamped; therefore, it will respond to actuating electrode commands with spurious, high frequency transients. Pressurizing the membrane vessel will introduce damping and reduce these transients (most membrane mirrors have operated at room air pressure, without specific control of the pressure). Air damping increases the response time of the mirror. Grosso and Yellin found an optimum pressure of 2 Torr (15 Pa) for their membrane mirror vessel using an experimental technique; at this pressure, their device reached equilibrium within approximately 100-200 μs of actuating electrode commands [32]. Flexible Optical BV (OKO Technologies) mirrors, operating at room air pressure, have response times approximately greater than 500 μs [36].

4.7 Control

Control of a membrane mirror in an adaptive optics system may have either of two broad objectives. The mirror may be commanded to a predetermined shape, such as a Zernike polynomial, in order to generate a desired wavefront. Alternatively, the mirror may be commanded to deform in response to signals generated from a wavefront sensor, which is full, closed loop adaptive optics.

With commonly used control or wavefront reconstruction algorithms, each of these objectives requires knowledge of the deformable mirror influence functions. Analytical calculation of the influence functions of a membrane deformable mirror in the linear approximation was performed in [56]. A numerical calculation of the influence functions for the more general, nonlinear case was developed in [57]. As discussed in Section 4.8, several groups have used Flexible Optical BV (OKO Technologies) mirrors in conjunction with wavefront sensors to empirically determine the influence functions in a calibration step, as part of specific adaptive optics applications.

A membrane mirror can be controlled without explicitly determining influence functions or reconstructing the wavefront. A synergy exists between common wavefront sensing schemes and the control requirements of a membrane mirror. As the name implies, curvature sensing measures the curvature of the wavefront, whereas voltages commanded to a membrane mirror control this curvature, through the Poisson equation. Thus data from a curvature sensor yields the required actuating voltages without numerically costly wavefront reconstruction. Similarly, Shack-Hartmann wavefront sensors measure the gradient of the phase, whose divergence gives the Laplacian. Thus the result of a simple divergence operation is directly proportional to the desired control signals to deform the membrane mirror to exactly the opposite, compensating curvature.

However, this control scheme cannot reproduce wavefronts with identically zero Laplacian, such as certain Zernike polynomials. Compensation of such terms requires control of the membrane mirror at its boundary, for example via actuating electrodes outside the active optical area [58].

4.8 Production of High Spatial Frequency Corrections

In order to ascertain the fundamental limitations of membrane mirrors, their ability to deform to shapes with high spatial frequency must be understood. Factors that affect the stroke of membrane mirrors at high spatial frequencies include

(i) Mechanics of membrane deformation
(ii) Limitation imposed by pre-bias curvature (if applicable)
(iii) Number of actuating electrodes
(iv) Diameter of the active optical area in comparison to the overall membrane diameter.

(i) Dimensional arguments and experience with numerical simulations suggest that amplitude of membrane deformation follows a –2 power law dependence on membrane spatial frequency. The membrane deforms according to Equation [1]. The response of the mirror as a function of spatial frequency may be estimated by inserting into the right hand side of Equation [1] a sinusoidally varying factor, $P/T = A\, e^{i\mathbf{k}\cdot\mathbf{r}}$, corresponding to the pressure distribution required to generate a mirror shape with spatial frequency, k. As a function of this spatial frequency, the mirror shape follows the power law $\xi(k) = A\, k^{-2}$, as can be seen by substitution into Equation [1]. The amplitude, $A = |P/T|$, is membrane dependent. Increasing the actuator pressure or decreasing the membrane tension can alter the spatial frequency response, as illustrated in Figure 4. According to these equations, membrane mirrors may be designed with considerable high frequency response, compared to existing designs such as the Flexible Optical BV (OKO Technologies) mirrors.

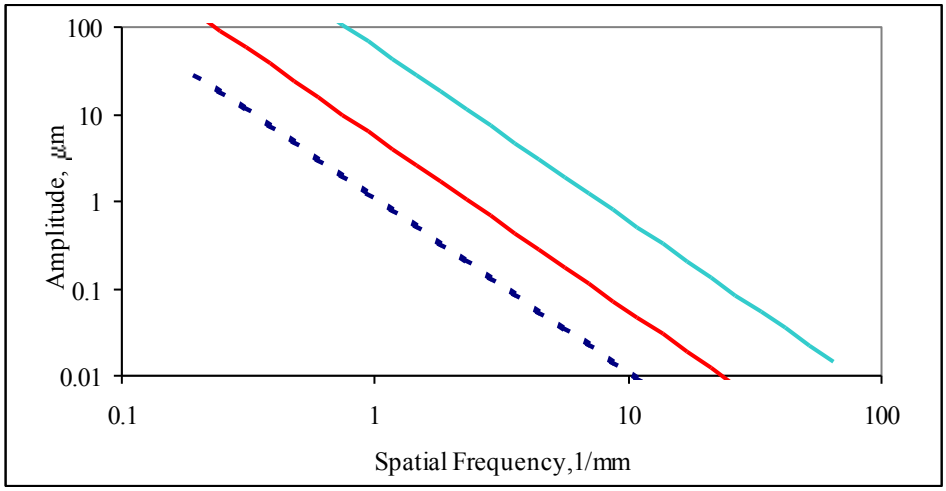

Figure 4. Membrane response as a function of spatial frequency varies as a power law. Dashed curve illustrates the response spectrum of a membrane with properties similar to a Flexible Optical BV (OKO Technologies) mirror. Middle curve illustrates the response of a lower stress membrane operated at higher voltage (20 MPa, 200 V). Top curve illustrates the response of the prototype bound charge membrane discussed in Section 5.

In a Monte Carlo simulation, Paterson, Munro and Dainty addressed the capability of the membrane mirror to correct for atmospheric turbulence, characterized by a $S(k) \sim k^{-11/6}$ spatial frequency spectrum [39]. Strehl ratios of 0.7 were achieved with the 37 actuator Flexible Optical BV (OKO Technologies) mirror. The close agreement between the membrane response spectrum and the aberration spectrum ($2 \approx 11/6$) suggests that membranes may be well suited to correct for atmospheric turbulence.

Experiments by Tyson and Frazier demonstrated that the 37 actuator Flexible Optical BV (OKO Technologies) membrane mirror was able to generate aberrations with a scaling law characteristic of atmospheric turbulence over the central part of the membrane [41]. These experiments and simulations suggest that when the optical pupil is confined to the central part of the membrane, the membrane is well suited to correct for aberrations with the spatial frequency distribution of atmospheric turbulence.

In a vision science adaptive optics system, Zhu et al. demonstrated a maximum mirror deflection of 7 μm, and they reproduced 20 Zernike modes (Zernike order n=0-5) using 37 actuators of the Flexible Optical BV (OKO Technologies) deformable mirror [42]. They generated wavefronts with 2.40 μm (3.5λ) peak to valley amplitudes, corresponding to a mirror stroke of 1.20 μm, for low order Zernike modes, and 1.37 μm (2.0λ) peak to valley amplitude wavefronts, corresponding to a mirror stroke of 0.685 μm, for higher order Zernike modes. Lower order Zernike modes were reproduced with good accuracy. Comparison of this data with Figure 1, and the data from Table 1, illustrates that this mirror stroke is nearly sufficient to correct for aberrations in human vision at each Zernike order.

(ii) Membrane mirrors that do not provide a restoring force experience an additional limitation to their spatial frequency response. These mirrors are pre-biased to a constant curvature; actuating electrodes can effectively repel the membrane mirror by releasing this bias voltage. The pre-bias curvature imposes an upper limit on the response spectrum. Scaling relations between maximum amplitude of correction and spatial frequency for such curvature limited membranes are presented in [52]. This limitation can be alleviated provided the membrane mirror has a restoring force, for example one approach is discussed in Section 5.

(iii) and (iv) can be addressed in future designs by including more electrodes under a larger (in proportion to the optical pupil) membrane, as discussed in Section 4.5.

5. BOUND CHARGE MEMBRANE MIRROR CONCEPT

Electrostatic actuation in a simple conducting membrane-electrode capacitor can only attract the membrane toward an electrode. Furthermore, the nonlinear dependence of pressure on the electrode voltage, as illustrated in Equation [3], and its dependence on the membrane-electrode distance, complicate the control and wavefront reconstruction problems. Addition of a bound charge layer to the membrane can resolve these difficulties, and present other advantages.

Permanently charged dielectrics have been used extensively in electret microphones [59]. Principles of design, and methods of charging electrets are discussed in [60]. These devices typically consist of a 12-25 μm Teflon TFE or FEP layer with a metal electrode deposited on one surface. The nonmetallized surface is placed 10-30 μm from a backplate electrode. Acoustic pressure from sound waves deforms the dielectric membrane and generates a signal voltage.

Corona discharge in a DC electric field may be used to implant charge into a dielectric. Insulating materials such as Teflon FEP may hold charge densities from 10^{-7}-10^{-9} C/cm^2 for many years under a variety of conditions. Charge has been stored in other materials including silicon dioxide.

5.1 Principle of Operation

The charged membrane mirror is schematically illustrated in Figure 5. The membrane is supported between two electrode planes, and has a dielectric coating on its top surface for reflectivity. A variant of this design might use a metallized membrane that is either at floating potential (realistically, connected to ground by some large resistance), or connected to a large capacitor for storing charge on the membrane in a quasi-permanent fashion.

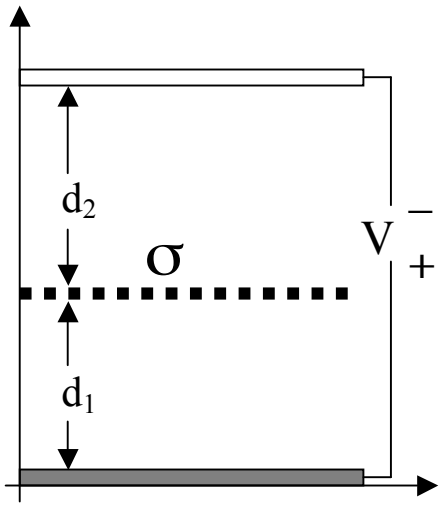

Figure 5. Schematic diagram of the bound charge membrane mirror. The mirror, represented by a dashed line, is suspended between a transparent electrode (top) and a plane of actuating electrodes (bottom). This diagram illustrates a single electrode, set to a voltage, *V*. The dielectric membrane has a permanent charge density, σ, and is held under tension at its periphery (not shown).

The top, transparent electrode is in the optical path, and is a ground connection. This electrode serves to define the electric field geometry, and might be replaced by an arrangement such as a ring, that does not obstruct the optical path. The bottom, actuating electrode is at a voltage, *V*. The membrane is at a distance d_1 from the actuating electrode and d_2 from the top electrode.

The electrostatic pressure on the membrane can be found from analysis of the electric fields on either side of the membrane. This pressure depends on two terms, one linear in the applied voltage, and one independent of the voltage.

Let E_1 and E_2 represent the electric fields on the bottom and top of the membrane, respectively. Electric fields are assumed to depend only on vertical distance. Let the membrane have a charge per unit area, σ, and negligible thickness. Equations for E_1 and E_2 can be found by applying Gauss's Law at the membrane surface, and conservation of energy between the electrodes:

$$E_2 - E_1 = \frac{\sigma}{\varepsilon_0} \quad [6]$$

$$E_1 d_1 + E_2 d_2 = V \quad [7]$$

Solving this system of equations yields

$$E_1 = \frac{V - \frac{\sigma d_2}{\varepsilon_0}}{D} \qquad E_2 = \frac{V + \frac{\sigma d_1}{\varepsilon_0}}{D} \quad [8a,b]$$

where $D \equiv d_1 + d_2$ is the total distance between the electrodes. The electrostatic pressure experienced by the membrane is proportional to the average electric field and the charge density,

$$P = \sigma \frac{1}{2}\left(E_1 + E_2\right) \quad [9]$$

Inserting Equations [8a,b] into Equation [9] yields a formula for the pressure in terms of the device parameters

$$P = \sigma \frac{V}{D} - \frac{\sigma^2 \left(d_2 - d_1\right)}{2\varepsilon_0 D} \quad [10]$$

5.2 Features of the Charged Membrane Mirror

First, consider the case where the membrane is equidistant from the electrodes, and the second term in Equation [10] vanishes (strictly only for small displacements of the membrane, as discussed below). The remaining term is linear in the applied voltage, V, and hence the pressure may change sign depending on the sign of the voltage. As a result, the membrane can experience either attraction or repulsion from the bottom electrode. Furthermore, this term depends on the constant, total distance between the electrodes. Unlike the more usual case of electrostatic actuation, where pressure varies with the inverse square of the distance from the membrane to the electrode, this constant term does not dominate the dynamics at very short distances. As a result, the device is not subject to the 1/3 gap instability normally encountered in electrostatic actuation. The membrane-electrode spacing may be minimized, in order to maximize the actuating pressure for a given, available voltage range.

The bound charge membrane is easier to deform than an ordinary, uncharged conducting membrane. An electrode charged to V=100V, acting on a membrane with a charge density $\sigma = 10^{-8}$ C/cm^2 and an electrode spacing D=50 μm yields an electrostatic pressure of 200 Pa, assuming the membrane is equidistant from either electrode. In comparison, the uncharged, conducting membrane experiences an electrostatic pressure given by Equation [2]

$$P = \frac{1}{2}\varepsilon_0 \frac{V^2}{d^2} \quad [11]$$

which yields P=70 Pa, under the same conditions (membrane-electrode spacing, d=25 μm, and electrode voltage V=100V).

To estimate the stroke achievable with this increased pressure, Equation [1] was solved under similar conditions as described in Section 4.4. In this case, a 10 μm thick circular membrane (thicker to allow for the bound charge layer and

a reflective, dielectric coating), fabricated with 15 MPa stress, has a tension T=150 N/m. Were such a membrane charged to 10^{-7} C/cm^2, located 40 μm from the actuating electrode, and actuated with V=100 V it would experience an electrostatic pressure of 1.2 kPa, from Equation [10]. From solving Equation [1] with these parameters, the membrane would have a maximum stroke of ± 4.5 μm due to a single, centered electrode, radius = 1/18 membrane radius. In comparison with the example from Section 4.4, the bound charge membrane exhibits the same total stroke at only half the actuating voltage.

Neglecting the second term in the expression for the pressure, Equation [10], is an approximation that is valid only for small displacements of the membrane. $d_2 - d_1$ is the displacement of the membrane from its undeflected position, ξ, using the notation from Section 4.2. Substituting Equation [10] into Equation [1] and re-arranging terms yields the general equation for static equilibrium of the membrane

$$\left(\nabla^2 + A \right)\xi = B \qquad [12]$$

$$A \equiv \frac{\sigma^2}{2\varepsilon_0 DT} \qquad B \equiv -\frac{\sigma V}{TD} \qquad [13a,b]$$

Equation [12] is a linear equation, in contrast to the non-linear Equation [3] for an uncharged, conducting membrane. Hence it is easier to solve under more general conditions, and this feature adds a further simplification to the control a charged membrane mirror.

The charged membrane may be intentionally located asymmetrically ($d_1 \neq d_2$) to load the membrane with a constant (actuator independent) pressure according to Equation [10]. Under this constant, lateral pressure, a circular membrane deforms to a paraboloid. By tuning the electrode offset, d_1-d_2, the focal length of the mirror may be set advantageously, for example to correct for an average, expected defocus from the wavefronts under consideration. Unlike the case of pre-biasing a conventional membrane mirror, this bias curvature does not limit the range of motion of the mirror, e.g. the maximum amplitude of deformation at high spatial frequencies. The mirror can be positively actuated in either direction, independent of any bias curvature. Pre-biasing the charged membrane mirror "conserves stroke" and increases its range of spatial frequency correction.

CONCLUSION

Deformable mirrors for vision science adaptive optics applications should have relatively large stroke compared to other adaptive optics deformable mirrors. Mirrors should be comparable in size to the human pupil, and feature several hundred degrees of freedom. They need not operate at the high frequencies of atmospheric compensation systems; therefore, vision science adaptive optics correctors can tolerate relatively low resonance frequencies. These requirements can be matched, and to some extent have already been demonstrated, by membrane deformable mirrors. Advances to membrane mirror technology may include designs that will actuate the membrane in both directions with respect to the electrode, and membranes that are fabricated with relatively low stress. Each of these factors will enable greater membrane mirror stroke at high spatial frequencies.

One such innovation to membrane mirrors has been presented. This design concept utilizes a permanent electrostatically charged membrane, in a well defined electric field configuration, to enable actuation in both directions with respect to electrodes. The response of such a membrane would be linear in the applied voltage, and would present other advantages over traditional membrane mirrors.

ACKNOWLEDGEMENTS

The authors wish to thank the following researchers for providing insightful comments, suggestions and assistance: Vladimir Aksyuk, Pablo Artal, Paul Bierden, Nathan Doble, Michael Helmbrecht, Bob Hufnagel, Howard Katz, Justin

Mansell, Don Miller, Gleb Vdovin, Jim West, Scott Wilks, Huawei Zhao. This work has been supported by the National Science Foundation Science and Technology Center for Adaptive Optics, managed by the University of California at Santa Cruz under cooperative agreement No. AST – 9876783.

REFERENCES

1. J. Liang, D. R. Williams and D. T. Miller, "Supernormal vision and high-resolution retinal imaging through adaptive optics," *J. Opt. Soc. Am.* Vol. 14 No. l 1, pp. 2884-2892, 1997.
2. D. Williams et al., "Wavefront Sensing and Compensation for the Human Eye," in *Adaptive Optics Engineering Handbook* ed. R. K. Tyson, pp. 287-310, Marcel Dekker, Inc., New York, 2000.
3. D. T. Miller, "Retinal Imaging and Vision at the Frontiers of Adaptive Optics," *Physics Today*, pp. 31-36, January 2000.
4. A. Roorda and D. R. Williams, "The arrangement of the three cone classes in the living human eye," *Nature* 397 pp. 520-522, 1999.
5. D. R. Williams et al., "How Far Can We Extend the Limits of Human Vision" in Customized Corneal Ablation: The Quest for Super Vision ed. S. MacRae et al., Slack Inc., Thorfare, NJ, 2001.
6. G.V. Schilling, "Adaptive Optics Comes of Age," *Sky & Telescope*, pp.30-40, October 2001.
7. J. W. Hardy, "Adaptive Optics," *Scientific American,* pp. 60-65, 1994.
8. R. Q. Fugate and W. W. Wild, "Untwinkling the Stars-Part 1," *Sky and Telescope,* pp. 24-31, May 1994.
9. R. Q. Fugate and W. W. Wild, "Untwinkling the Stars-Part 2," *Sky and Telescope,* pp. 20-27, June 1994.
10 J. Liang and D. R. Williams, "Aberrations and retinal image quality of the normal human eye," *J. Opt. Sci. Am. A*., Vol. 14 No. 11, pp. 2873-2883, 1997.
11. J. M. Geary, "Wavefront Sensors," *Adaptive Optics Engineering Handbook*, R. K. Tyson, pp. 123-150, Marcel Dekker, Inc., New York, 2000.
12. F. Roddier, "Curvature Sensing and Compensation," *Applied Optics* Vol. 27, pp 1223-1225, 1998.
13. R. E. Aldrich, "Deformable Mirror Wavefront Correctors," *Adaptive Optics Engineering Handbook*, R. K. Tyson, pp. 151-197, Marcel Dekker, Inc., New York, 2000.
14. G. D. Love, "Liquid Crystal Adaptive Optics," *Adaptive Optics Engineering Handbook*, R. K. Tyson, pp. 151-197, Marcel Dekker, Inc., New York, 2000.
15. M. A. Ealey and J. A. Wellman, "Deformable Mirrors: Design Fundamentals, Key Performance Specifications, and Parametric Trades," *SPIE* Vol. 1543, pp. 36-51, 1991.
16. Gosselin, P. et al., "Objective Comparisons between Stacked Array Mirror and Bimorph Mirrors," *SPIE* Vol. 1920, pp. 81
17. R. Mali et al., "Development of microelectromechanical deformable mirrors for phase modulation of light," *Optical Engineering,* Vol. 36 No. 2, pp. 542-548, 1997.
18. J. D. Mansell et al., "Silicon Deformable Mirrors and CMOS-based Wavefront Sensors," SPIE Vol. 4124, 2000.
19. W. D. Cowan and V. M. Bright, "Surface Micromachined Deformable Mirrors," *Adaptive Optics Engineering Handbook*, R. K. Tyson, pp. 249-272, Marcel Dekker, Inc., New York, 2000.
20. P. Jagourel et al., "Adaptive Optics: a bimorph mirror for wavefront correction," *SPIE* Vol. 1237 pp. 394, 1990.
21. M. Roggerman et al., "Use of micro-electro-mechanical deformable mirrors to control aberrations in optical systems: theoretical and experimental results," *Optical Engineering*, Vol. 36 No. 5, pp. 1326-1338, 1997.
22. W. D. Cowan et al., "Optical phase modulation using a refractive lenslet array and microelectromechanical deformable mirror," *Optical Engineering*, Vol. 37 No. 12, pp. 3237-3247, 1998.
23. B. Hulburd and D. Sandler, "Segmented mirrors for atmospheric compensation," *Optical Engineering*, Vol. 29 No. 10, pp. 1186-1190, 1990.
24. W. D. Cowan et al, "Evaluation of microfabricated deformable mirror systems," *SPIE* Vol. 3353, pp. 790-804, 1998.
25. M. A. Michalicek et al., "Design and simulation of advanced surface micromachined micromirror devices for telescope adaptive optics applications," *SPIE* Vol. 3353, pp. 805-815, 1998.
26. M. A. Helmbrecht et al., "Micromirrors for Adaptive-Optics Arrays," presented at Transducers 2001.
27. U. Srinivasan et al., "Fluidic Self Assembly of Micromirrors onto Surface Micromachined Actuators," *Proc. 2000 IEEE/LEOS Intl. Conf. on Optical MEMS*, Kauai, HI, pp. 59-60, 2000.
28. H. Zhao, Indiana University, private communication, July 2001

29. D. T. Miller, X. Hong and L. Thibos, "Requirements for segmented spatial light modulators for diffraction-limited imaging through aberrated eyes" in *Proceedings of the 2nd International Workshop on Adaptive Optics in Industry and Medicine* ed. G.D. Love p. 63, World Scientific, Singapore, 1999.
30. J. W. Hardy, *Adaptive Optics for Astronomical Telescopes,* p. 195, Oxford University, New York, 1998.
31. D. Fried, "Adaptive Optics Development: A 30 Year Personal Perspective." Talk presented at Lawrence Livermore National Laboratory, April 30, 2001.
32. R. P. Grosso and M. Yellin, "Membrane mirror as an adaptive optical element," *J. Opt. Sci. Am*. Vol. 67, pp. 399, 1977.
33. R.M. Centamore and A. Wirth, "High Bias Membrane Mirror," *SPIE Vol. 1543 Active & Adaptive Optical Components,* pp. 128-132, 1991.
34. H. Takami and M. Iye, "Membrane deformable mirror for SUBARU adaptive optics," *SPIE Vol. 2201 Adaptive Optics in Astronomy*, pp. 762-767, 1994.
35. G. S. Burley, J. R. Stilburn, G. A. H. Walker, "Membrane mirror and bias electronics," *Applied Optics* Vol. 37 No. 21, pp. 4649-4655, 1998.
36. G. Vdovin, and P. M. Sarro, "Flexible mirror micromachined in silicon," *Applied Opt*ics Vol. 34, pp. 2968-2972, 1995.
37. L. Zhu et al., "Adaptive control of a micromachined continuous-membrane deformable mirror for aberration compensation," *Applied Optics* Vol. 38 No. 1, pp 168-178, 1999.
38. I. Iglesias and P. Artal, "Closed loop adaptive optics in the human eye," *Optics Letters* Vol. 26 No. 10 pp. 746-748, 2001.
39. C. Paterson, I. Munro and J. C. Dainty, "A low cost adaptive optics system using a membrane mirror," *Optics Express* Vol. 6 No. 9, pp 175-185, 2000.
40. O. Albert, et al., "Smart microscope: an adaptive optics learning system for aberration correction in multiphoton confocal microscopy," *Optics Letters* Vol. 25 No. 1, pp52-54, 2000.
41. R. K. Tyson and B. W. Frazier, "Microelectromechanical system programableaberration generator for adaptive optics," *Applied Optics* Vol. 40 No. 13, pp. 2063-2067, 2001.
42. L. Zhu et al., "Wave-front generation of Zernike polynomial modes with a micromachined membrane deformable mirror*" Applied Optics* Vol. 38 No. 28 pp. 6019-6026, 1999.
43. L. M. Miller et al., "Fabrication and characterization of a micromachined deformable mirror for adaptive optics applications," *SPIE* Vol. 1945, pp. 421-430, 1993.
44. J. D. Mansell et al., "Micromachined Silicon Deformable Mirror," *SPIE* Vol. 3353, pp. 896-901, 1998.
45. G. Vdovin and V. Kiyko, "Intracavity control of a 200-W continuous-wave Nd:YAG laser by a micromachined deformable mirror," *Optics Letters* Vol. 26 No. 11, pp. 798-800, 2001.
46. C. Divoux et al., "Miniaturized Deformable Magnetic Mirror for Adaptive Optics," SPIE Vol. 3353 *Conference on Adaptive Optical Systems Technologies*, pp. 850-857, 1998.
47. O. Cugat et al., "Deformable magnetic mirror for adaptive optics: technological aspects." *Sensors and Actuators A* Vol. 89, pp. 1-9, 2001.
48. W. D. Cowan et al., "Evaluation of microfabricated deformable mirror systems," *SPIE*, Vol. 3353, pp. 790-804, March 1998.
49. S. Timoshenko and S. Woinowsky-Krieger, *Theory of Plates and Shells*, McGraw-Hill Book Co. Inc., New York, 1959
50. L. D. Landau and E. M. Lifshitz, *Theory of Elasticity Course in Theoretical Physics Vol. 7,* Butterworth-Heineman, Boston, 1959.
51. ibid., p. 52, Eq. 14-4.
52. G. Vdovin, "Micromachined Membrane Deformable Mirrors," in *Adaptive Optics Engineering Handbook* ed. R. K. Tyson, p. 237, Marcel-Dekker, Inc., New York, 2000.
53. P.K.C. Wang, R. C. Gutierrez, R. K. Bartman "A method for designinig electrostatic-actuator electrode pattern in micromachined deformable mirrors" Sensors and Actuators A Vol. 55, pp. 211-217, 1996.
54. P. M. Morse, *Vibration and Sound, 2nd Ed*., p. 118, McGraw-Hill Book Co., New York, 1948.
55. L. E. Kinsler, and A. R. Frey, *Fundamentals of Acoustics 2nd Ed*., p. 191, John Wiley & Sons Inc., New York, 1948.

56. E. S. Claflin and N. Baraket "Configuring an electrostatic membrane mirror by least squares fitting with analytically derived influence functions," *J. Opt. Sci. Am. A* Vol. 3 No. 11, pp. 1833-1839, 1986.
57. P.K.C. Wang and F. Y. Hadaegh, "Computation of Static Shapes and Voltages for Micromachined Deformable Mirrors with Nonlinear Electrostatic Actuators," *JMEMS* Vol. 5 No. 3, pp. 205-220, 1996.
58. Bob Hufnagel, private communication, April 2001.
59. G. M. Sessler and J.E. West, "Applications" in *Electrets* ed. G. M. Sessler, pp. 347-379, Springer-Verlag, New York, 1987.
60. G. M. Sessler, "Physical Principles of Electrets," in *Electrets* ed. G. M. Sessler, pp. 13-75, Springer-Verlag, New York, 1987.